DOI: 10.1002/ejic.200600403

Controlled Synthesis of 3d–4d Heterobimetallic Complexes of a Symmetrical Tetraiminodiphenolate Macrocycle – Structural, Spectroscopic, and Redox Properties

Bula Dutta,[a] Bibhutosh Adhikary,[b] Ulrich Flörke,[c] and Kamalaksha Nag*[a]

Keywords: Heterobimetallic complexes / Macrocyclic complexes / Palladium / Rhodium / 3d metals(II)

The mononuclear complexes $[Rh(LH_2)Cl_2](ClO_4)\cdot 3H_2O$ (**1**) and $[Pd(LH_2)](ClO_4)_2$ (**2**) of the tetraiminodiphenolate macrocycle L^{2-} have been synthesized by the transmetallation reaction between $[Pb(LH_2)](ClO_4)_2$, and $RhCl_3\cdot xH_2O$ and $Na_2[PdCl_4]$, respectively. In these compounds, the uncoordinated imino nitrogen atoms are protonated and are hydrogen bonded to the phenolate oxygen atoms to stabilize them against hydrolytic cleavage. Using these mononuclear complexes, the following heterodinuclear complexes: $[Rh^{III}Cl_2(L)Pd^{II}](X)$ [X = ClO_4 (**3**), PF_6 (**4**)], $[Pd^{II}(L)M^{II}(H_2O)_2](ClO_4)_2$ [M = Mn (**5**), Fe (**6**), Co (**7**), Ni (**8**)], $[Pd^{II}(L)M^{II}](ClO_4)_2$ [M = Cu (**9**), Zn (**10**)]; and the dipalladium(II) complex $[Pd_2L](ClO_4)_2$ (**11**) have been synthesized. The crystal structure determined for $[RhCl_2(L)Pd](PF_6)$ (**4**) shows an axially elongated octahedral geometry for Rh^{III} and a square-planar geometry for Pd^{II}. In $[Pd^{II}(L)Cu^{II}](ClO_4)_2$ (**9**), both the metal ions lie in the flat plane of the macrocyclic ligand and they are positionally disordered with equal occupancies. The Cu^{II} center has an apically elongated square-pyramidal geometry due to the weak perturbation by an oxygen atom of a perchlorate anion. Complexes **2**, **10**, and **11** on excitation at 400 nm exhibit luminescence at room temperature at 505, 437, and 443 nm, respectively. Spectrofluorimetric titrations of $[Pd^{II}(LH_2)]^{2+}$ with the acetate salts of zinc(II) and palladium(II) have shown that the formation of $[Pd(L)Zn]^{2+}$ and $[Pd_2L]^{2+}$ complex species are accompanied by blue shift of luminescence with increased and reduced emission intensities, respectively. The hyperfine-shifted ^1H NMR spectral features of the paramagnetic compounds **7**–**9** have been analyzed by determining their longitudinal (T_1) and transverse (T_2) relaxation times. Cyclic and square-wave voltammetric measurements have been carried out for complexes **7**–**9** in acetonitrile. For complexes **8** and **9**, reversible one-electron reduction occurs with $E_{1/2}$ = –0.10 V for $Pd^{II}Cu^{II}/Pd^{II}Cu^{I}$ and –0.80 V for $Pd^{II}Ni^{II}/Pd^{II}Ni^{I}$ versus Ag/AgCl. Complex **7** undergoes irreversible reduction for cobalt(II) at –0.78 V.

Introduction

Over the past three decades extensive studies have been made on the chemistry of the phenolate-bridged tetraiminodiphenol macrocyclic complexes[1–17] derived from the symmetrical ligand L^{2-} (**I**). The focus of interest in complexes of this sort has been to study the implications of cooperative metal–metal interactions that are manifested in spin-exchange couplings,[6–15] redox activities,[4,8,9a,11] and bimetallic reactivities.[9b,16]

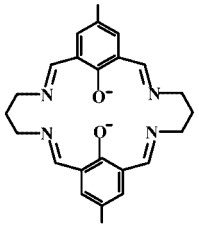

I (L^{2-})

There is considerable interest in involving heterobimetallic complexes in catalytic reactions by way of dual activation of substrates.[18–20] Heterobimetallic complexes also have distinct potentiality to act as precursors for producing bimetallic nanoparticles, especially those containing platinum metals and first-row transition metals.[21] The synthesis of heterobimetallic complexes where the two metal ions are held in close proximity by a bridging ligand is a nontrivial problem, particularly when the ligand is symmetrical in nature. The most common problem in such cases is either the preferential formation of a particular homodinuclear complex species or the statistical formation of a mixture of two products. Clearly, the development of a controlled synthetic route for the generation of heterobimetallic complexes is an important task. We have introduced a controlled systematic route to synthesize bimetallic systems of the symmetric

[a] Department of Inorganic Chemistry, Indian Association for the Cultivation of Science,
Jadavpur, Kolkata 700 032, India
E-mail: ickn@iacs.res.in
[b] Department of Chemistry, Bengal Engineering and Science University,
Shibpur, Howrah 711 103, India
[c] Anorganische und Analytische Chemie, Universität Paderborn, 33098 Paderborn, Germany

Supporting information for this article is available on the WWW under http://www.eurjic.org or from the author.

macrocyclic ligand L^{2-} incorporating 4d–3d metal ions. Herein we report the synthesis, structures, and spectroscopic properties of the mononuclear complexes $[M(LH_2)]^{n+}$ ($M = Rh^{III}$, Pd^{II}; $n = 3$, 2) and the heterodinuclear complexes $[RhCl_2(L)Pd]^+$ and $[Pd(L)M]^{2+}$ ($M = Mn^{II}$, Fe^{II}, Co^{II}, Ni^{II}, Cu^{II}, Zn^{II}). The X-ray crystal structures of two heterodinuclear complexes $[RhCl_2(L)Pd](PF_6)$ and $[Pd(L)Cu](ClO_4)_2$ have been determined. Paramagnetic proton NMR studies have provided information about the influence of electron spins on the hyperfine-shifted spectral patterns of $[Pd(L)M^{II}]^{2+}$ (M = Fe, Co, Ni, Cu) complexes.

Results and Discussion

Syntheses

The synthesis of heterobimetallic complexes involving 3d–4d metal ions and the symmetrical compartmental macrocyclic ligand L^{2-} would ideally require mononuclear precursor complexes in which one compartment of the ligand is metal-free. However, for the ligand L^{2-} such mononuclear complexes are generally not obtainable.[1,2,5,16b] It has been reported[22] that metal-directed macrocyclization usually does not take place with nonlabile platinum metals. Indeed, we have failed to produce mononuclear or dinuclear complexes of palladium(II) and rhodium(III) of L^{2-} through a [2+2] condensation reaction between 2,6-diformyl-4-methylphenol and 1,3-diaminopropane in the presence of $Na_2[PdCl_4]$ or $RhCl_3{\cdot}xH_2O$. In both cases, a mixture of reaction products was obtained which consisted of, inter alia, amine aldehyde condensed oligomers, metal diamine complexes, and $[Pd_2L']$ or $[RhL'(H_2O)Cl]$ where H_2L' is the [2+1] Schiff base of 2,6-diformyl-4-methylphenol and 1,3-diaminopropane.

To obviate this problem, sometime back we reported the synthesis of a mononuclear lead(II) complex, $[Pb(LH_2)](ClO_4)_2$,[23] by reacting 1 equiv. of lead perchlorate with 2 equiv. each of 2,6-diformyl-4-methylphenol and 1,3-diaminopropane in the presence of acetic acid. In this complex, LH_2 represents the macrocycle in the zwitterionic form in which the two uncoordinated imine nitrogens are protonated and are hydrogen-bonded to the metal-bound phenolate oxygens. The utility of $[Pb(LH_2)](ClO_4)_2$ as a precursor to obtain other mononuclear complexes has been demonstrated by us[24] by isolating complexes $[M^{III}(LH_2)(H_2O)Cl](ClO_4)_2{\cdot}nH_2O$ of trivalent labile metal ions such as aluminum, gallium, and indium.

As shown in Scheme 1, the metathetical reaction involving stoichiometric amounts of $[Pb(LH_2)](ClO_4)_2$ and $RhCl_3{\cdot}xH_2O$ or $Na_2[PdCl_4]$ and excess $NaClO_4$ leads to the formation of $[Rh(LH_2)Cl_2](ClO_4){\cdot}3H_2O$ (**1**) and $[Pd(LH_2)](ClO_4)_2$ (**2**). The driving force for the reaction is precipitation of $PbCl_2$ and occupation of its vacant site by rhodium(III) or palladium(II). The palladium(II) complex (**2**), on reaction with a stoichiometric amount of a 3d metal perchlorate $M(ClO_4)_2{\cdot}6H_2O$ (M = Mn, Fe, Co, Ni, Cu, Zn)

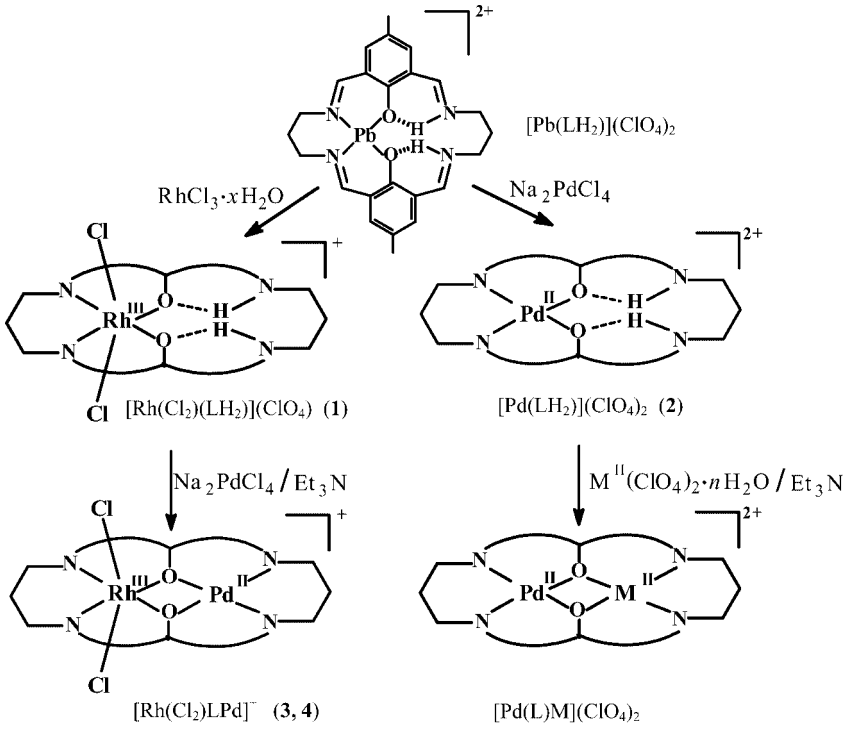

Scheme 1.

and triethylamine, affords the heterodinuclear complexes $[Pd(L)M(H_2O)_2](ClO_4)_2$ (**5**–**8**, Mn–Ni), $[Pd(L)Cu](ClO_4)_2$ (**9**), and $[Pd(L)Zn(H_2O)](ClO_4)_2{\cdot}H_2O$ (**10**). If the above reaction is carried out with $Na_2[PdCl_4]$ and $NaClO_4$, the homodinuclear complex $[Pd_2L](ClO_4)_2$ (**11**) is obtained. In contrast to **2**, the reaction of $[RhCl_2(LH_2)](ClO_4){\cdot}3H_2O$ (**1**) with the above-mentioned metal perchlorates, however, failed to produce the desired $[RhCl_2(L)M(H_2O)_n]^+$-type complexes. On the other hand, when **1** is reacted with $Na_2[PdCl_4]$ and triethylamine in the presence of $NaClO_4$ or $NH_4[PF_6]$ the mixed-metal $[RhCl_2(L)Pd](ClO_4)/(PF_6)$ complexes **3**, **4** are readily obtained. This indicates that the *trans* axial chloride ions of **1** sterically inhibit the entry of a second metal ion into the ligand compartment if the coordination number of the incoming metal ion exceeds four. In the case of palladium(II), no difficulty is encountered in obtaining $[RhCl_2(L)Pd]^+$ because of the square-planar geometry of the palladium center.

It needs to be mentioned at this stage that the dipalladium(II) complex $[Pd_2L](BF_4)_2$ has been prepared earlier[16a] by reacting the macrocyclic ligand salt $[H_4L](BF_4)_2$ with palladium(II) chloride or acetate in acetonitrile in the presence of a 10-fold excess of triethylamine. The X-ray crystal structure of this compound has been reported.[16a] Further, the heterodinuclear complex $[PdLNi(CH_3CN)_2](ClO_4)_2$ has been previously synthesized[25] by reacting the much earlier reported mononuclear nickel(II) complex $[Ni(H_2L)](ClO_4)_2{\cdot}H_2O$[1] with palladium(II) acetate in acetonitrile. This compound has also been structurally characterized.[25] We note that the proton NMR spectra reported for $[PdLNi(CH_3CN)_2]^{2+}$ in CD_3OD are similar to those of $[PdLNi(H_2O)_2]^{2+}$ in CD_3CN obtained in this study.

Crystal Structures

[Rh(Cl$_2$)(L)Pd]PF$_6$ (4)

The structural analysis of complex **4** revealed the presence of the core cation $[Pd(L)RhCl_2]^+$ and one hexafluorophosphate anion. An ORTEP representation of the cation $[Pd(L)RhCl_2]^+$ is shown in Figure 1 and selected interatomic distances and angles are listed in Table 1.

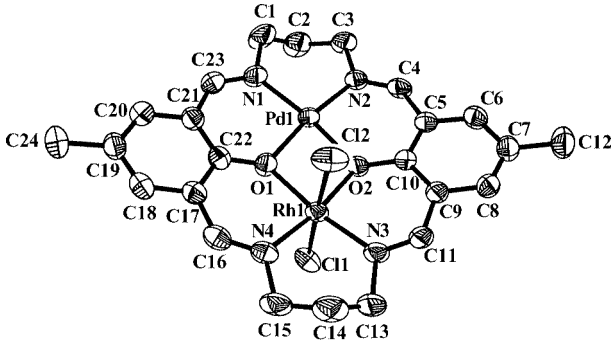

Figure 1. ORTEP representation of the $[Pd(L)Rh(Cl_2)]^+$ cation of complex **4** at the 50% probability level. H atoms omitted.

The structure of the cation of **4** consists of one palladium(II) and one rhodium(III) center bridged by the two phenolate oxygens O(1) and O(2) and they are separated by a distance of 3.150(1) Å. The dihedral angle between the two phenyl rings is 22.76(1)°, indicating significant deviation of the macrocycle from the planarity. For the Pd(1) center the basal plane is provided by the atoms O(1), O(2), N(1), and N(2) [Pd(1)–O(1) 2.022(2) Å, Pd(1)–O(2) 2.024(2) Å, Pd(1)–N(1) 1.980(3) Å, and Pd(1)–N(2) 1.990(3) Å]. These donor atoms are deviated from the mean plane by not more than ±0.010(1) Å and the Pd(1) center lies below the plane by 0.009(1) Å. The Rh(1) center is bonded to the phenolate oxygen atoms O(1) [Rh(1)–O(1) 2.056(2) Å] and O(2) [Rh(1)–O(2) 2.062(2) Å], and the imine nitrogen atoms N(3) [Rh(1)–N(3) 1.984(3) Å] and N(4) [Rh(1)–N(4) 2.001(3) Å]. The mean plane is formed by O(1), O(2), N(3), and N(4) atoms in which the deviations of the donor atoms do not exceed ±0.004(1) Å. The *trans* axial Cl(1) and Cl(2) atoms are placed above and below the metal plane to complete

Table 1. Selected bond lengths [Å] and angles [°] for $[RhCl_2(L)Pd](PF_6)$ (**4**).

Pd(1)–N(1)	1.980(3)	Rh(1)–N(3)	1.984(3)
Pd(1)–N(2)	1.990(3)	Rh(1)–N(4)	2.001(3)
Pd(1)–O(1)	2.022(2)	Rh(1)–O(1)	2.056(2)
Pd(1)–O(2)	2.024(2)	Rh(1)–O(2)	2.062(2)
		Rh(1)–Cl(1)	2.3395(13)
		Rh(1)–Cl(1)	2.3065(13)
N(1)–Pd(1)–N(2)	95.78(12)	N(3)–Rh(1)–N(4)	96.86(13)
N(1)–Pd(1)–O(1)	92.43(11)	N(3)–Rh(1)–O(1)	170.34(11)
N(2)–Pd(1)–O(1)	171.71(11)	N(4)–Rh(1)–O(1)	92.79(12)
N(1)–Pd(1)–O(2)	171.82(11)	N(3)–Rh(1)–O(2)	92.63(11)
N(2)–Pd(1)–O(2)	92.40(11)	N(4)–Rh(1)–O(2)	170.51(11)
O(1)–Pd(1)–O(2)	79.39(10)	O(1)–Rh(1)–O(2)	77.72(9)
		N(3)–Rh(1)–Cl(2)	89.58(10)
Pd(1)–O(1)–Rh(1)	101.12(11)	N(4)–Rh(1)–Cl(2)	91.10(10)
Pd(1)–O(2)–Rh(1)	100.88(10)	N(3)–Rh(1)–Cl(1)	89.06(10)
		N(4)–Rh(1)–Cl(1)	90.43(10)
		O(1)–Rh(1)–Cl(2)	89.82(9)
		O(2)–Rh(1)–Cl(2)	88.97(8)
		O(1)–Rh(1)–Cl(1)	91.29(9)
		O(2)–Rh(1)–Cl(1)	89.72(8)
		Cl(2)–Rh(1)–Cl(1)	178.07(4)

the octahedron. The two Rh–Cl distances [Rh(1)–Cl(1) 2.339(1) Å and Rh(1)–Cl(2) 2.306(1) Å] are almost the same, albeit rather long. The Cl(2)–Rh(1)–Cl(1) angle [178.07(4)°] is practically linear. The displacement of Rh(1) from the least-square plane is only 0.003(1) Å.

[Pd(L)Cu](ClO$_4$)$_2$ (9)

Compound **9** is comprised of the cation $[Pd(L)Cu]^{2+}$ and two perchlorate anions. The ORTEP view of the cation is shown in Figure 2. The relevant bond lengths and angles are given in Table 2. The $[Pd(L)Cu]^{2+}$ cation lies on a crystallographic inversion center and thus the M_2O_2 ring is planar with M = Pd and Cu centers disordered over both sites (site occupation factor 0.5). The two metal centers are bridged by the two phenolate oxygens O(1) and O(1A) and they are separated by a distance of 3.083(1) Å. The basal plane for either of the metal atoms is formed by the N_2O_2 donor atoms and the average metal–donor atom distances are M(1)–O(1) 1.965(4) Å, M(1)–O(1)#1 1.998(4) Å, M(1)–N(1) 1.997(5) Å, and M(1)–N(2) 1.971(6) Å. The deviation of the constituent N_2O_2 atoms from the mean plane is 0.024(1) Å and both the metal centers are equally displaced in opposite directions from the mean plane by 0.031(1) Å. The $[Pd(L)Cu]^{2+}$ cation is not perfectly flat, as the atoms C(2) and C(2A) are significantly off [0.62(1) Å] the mean cation plane. Moreover, the perchlorate anions are heavily disordered. The distance between the Cu center and a perchlorate oxygen O(14) is 2.54 Å. This Cu···O distance is not unusual for an apical perchlorate donor on otherwise square-planar copper(II).

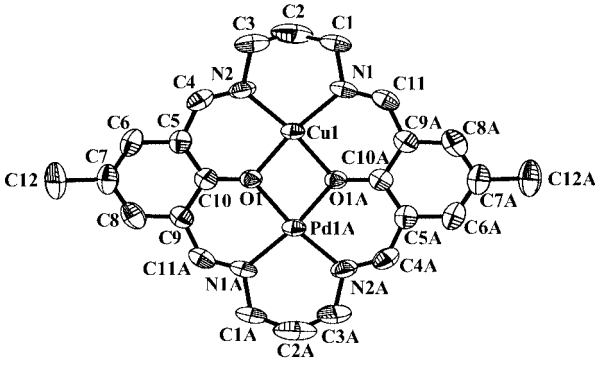

Figure 2. ORTEP representation of the $[Pd(L)Cu]^{2+}$ of complex **9** at the 50% probability level. H atoms omitted. "A" labels indicate symmetry-related atoms (–*x*, –*y* + 1, –*z* + 1).

It should be noted that 0.5:0.5 disorder of the palladium(II) and copper(II) centers over two sites might as well indicate that **9** is a 1:1 mixture of $[Pd_2L](ClO_4)_2$ and $[Cu_2L](ClO_4)_2$ rather than the mixed-metal complex $[Pd(L)Cu](ClO_4)_2$. However, it will be seen in the next section that the mass spectrum of **9** provides clear evidence that it is a truly heterodinuclear complex.

In this context it would be relevant to consider the crystal structures reported for the homodinuclear complexes of palladium(II) and copper(II). In $[Pd_2L](BF_4)_2 \cdot 2CH_3NO_2$,[16a] the average Pd–O, Pd–N, and Pd···Pd distances are 2.015(1), 1.987(6), and 3.1511(6) Å, respectively. The structure determined for the dicopper(II) complex $\{[Cu_2L(H_2O)_2(ClO_4)_2][Cu_2L(H_2O)_2](ClO_4)_2\}$[12b] showed the presence of two different complex units in the unit cell. In one of these units, the dicopper(II) centers are pseudo-octahedral because of *trans* axial coordination by the oxygen atoms of perchlorate and water and the relevant bond lengths are Cu–O 1.985(6) Å, Cu–N 1.956(8) Å, Cu–O(perchlorate) 2.589(10) Å, Cu–O(water) 2.451(9) Å, and Cu···Cu 3.091(3) Å. In the second unit, the copper(II) centers have square-pyramidal geometry with the following bond lengths: Cu–O 1.970(6) Å, Cu–N 1.965(9) Å, Cu–O(water) 2.451(6) Å, and Cu···Cu 3.096(3) Å. Further, in the first unit the copper center is displaced from the equatorial mean plane by only 0.019(4) Å, while in the second unit this displacement, 0.083(6) Å, is greater. A comparison of the structural geometries of the metal centers and the metrical parameters of **9** with the dipalladium(II) and dicopper(II) systems clearly reveals that **9** is a discrete compound.

Table 2. Selected bond lengths [Å] and angles [°] for [Pd(L)Cu](-ClO$_4$)$_2$ (**9**).

M(1)–O(1)	1.965(4)
M(1)–O(1)#	1.998(4)
M(1)–N(1)	1.997(5)
M(1)–N(2)	1.971(6)
M···M	3.0831(1)
O(1)–M(1)–N(2)	92.2(2)
O(1)–M(1)–N(1)	170.5(2)
N(1)–M(1)–N(2)	96.5(2)
O(1)–M(1)–O(1)#	77.86(19)
N(2)–M(1)–O(1)#	170.3(2)
N(1)–M(1)–O(1)#	92.7(2)
C(11)–N(1)–M(1)	122.8(4)
C(1)–N(1)–M(1)	122.9(5)
C(4)–N(2)–M(1)	123.3(5)
C(3)–N(2)–M(1)	120.4(6)

Mass Spectra

The electrospray ionization mass spectra (ESI positive) of complexes **1**–**11**, except for **5**, have been measured using their acetonitrile solutions (about 10^{-4} mol·dm^{-3}). The mononuclear complex **1** shows two peaks due to the cations $[Rh^{III}(Cl_2)(LH_2)]^+$ and $[Rh^{III}(Cl)(ClO_4)(LH_2)]^+$, whereas compound **2** shows peaks due to the cations $[Pd^{II}(LH_2)(ClO_4)]^+$ and $[Pd^{II}(LH_2)]^{2+}$. The heterodinuclear $Rh^{III}Pd^{II}$ compounds **3** and **4** show only a single peak due to the $[Rh^{III}(Cl_2)(L)Pd^{II}]^+$ cation.

For the heterodinuclear $Pd^{II}M^{II}$ complexes (M = Fe, Co, Ni, Cu, Zn) and the homodinuclear $Pd^{II}Pd^{II}$ complex similar spectral features have been observed. These are characterized by the occurrence of two types of positively charged species: $[Pd^{II}(L)M^{II}(ClO_4)]^+$ and $[Pd^{II}(L)M^{II}]^{2+}$, of which the doubly positive-charged ion forms the base peak. Figure 3 shows the cluster of peaks observed for the two types of molecular cations of **7** along with their corresponding simulated spectral patterns. It may be noted that the

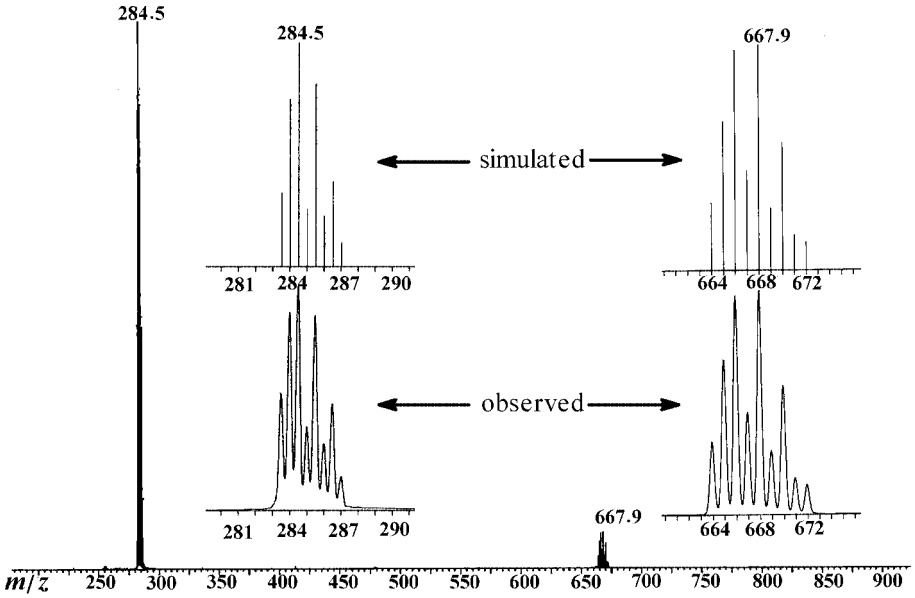

Figure 3. Electrospray ionization mass spectra (ESI-MS+) of $[Pd^{II}(L)Co^{II}](ClO_4)_2$ (**7**) in acetonitrile. Simulated isotropic spectral patterns are compared with the observed major positively charged cationic species.

number of peaks, *m*/*z* values, and the relative peak heights observed for the cations $[Pd^{II}(L)Co^{II}(ClO_4)]^+$ and $[Pd(L)Co]^{2+}$ are in excellent agreement with the calculated spectral patterns obtained by taking into consideration the relative abundances of the isotopes of the constituent elements.

The mass spectrum of the complex $[Pd(L)Cu](ClO_4)_2$ (**9**) has been of particular interest in this context because, as already noted, the X-ray structure of this compound raised the possibility of considering it as a mixture of $[Pd_2L](ClO_4)_2$ and $[Cu_2L](ClO_4)_2$. The spectrum of **9** (shown in Figure S1) depicts the presence of peaks only due to $[Pd(L)Cu(ClO_4)]^+$ with *m*/*z* = 671.9 (10%) and $[Pd(L)Cu]^{2+}$ with *m*/*z* = 287.5 (100%). The observed and calculated isotopic abundance ratio patterns of the positively charged species (see Figure S1, supporting information) are in excellent agreement with each other. Further, the total absence of peaks due to $[Pd_2(L)(ClO_4)]^+$ (715), $[Cu_2(L)(ClO_4)]^+$ (629), $[Pd_2(L)]^{2+}$ (309), and $[Cu_2(L)]^{2+}$ (265) rules out the possibility of **9** as a mixture of the two homodinuclear complexes.

Infrared Spectra

The IR spectroscopic data of complexes **1**–**11** are given in the Exp. Sect. The $\nu_{C=N}$ stretching vibrations of all the complexes lie between 1650 and 1630 cm^{-1}. For the mononuclear complexes **1**, **2** the $\nu_{C=N}$ vibration is observed at 1650 cm^{-1}, while for the dinuclear complexes **3**–**11** this band is shifted to lower energy, 1635–1630 cm^{-1}. In the mononuclear complexes, a weak band is observed at about 3150 cm^{-1} due to the protonated imine (ν_{NH}), which is hydrogen-bonded to the phenolate oxygen. As expected, this band is not observed in the dinuclear complexes.

Electronic Spectra

The electronic spectroscopic data for complexes **1**–**11** are listed in Table 3. The mononuclear complexes $[Rh(LH_2)Cl_2](ClO_4)\cdot 3H_2O$ (**1**) and $[Pd(LH_2)](ClO_4)_2$ (**2**) exhibit similar absorption spectral features with a relatively broad band around 406 nm and two intense bands around 260 nm and 220 nm. The latter two bands are due to intraligand charge transfer transitions, whereas the first one seems to be due to ligand (phenolate) to metal charge transfer (LMCT) transition. The spectral patterns observed for the heterodinuclear $Rh^{III}Pd^{II}$ complexes are again similar to those of **1** and **2**, although the LMCT band is shifted to 385 nm.

The heterodinuclear diamagnetic $Pd^{II}M$ (M = Zn, Pd) complexes **10**, **11** also exhibit spectral features as above (Table 3). Significant spectral changes occur when M^{II} is a transition-metal ion. For example, the absorption spectrum of the $Pd^{II}Co^{II}$ complex (**7**) (Figure S2) shows three bands at 970 nm (16 $dm^3\cdot mol^{-1}\cdot cm^{-1}$), 375 nm (36400 $dm^3\cdot mol^{-1}\cdot cm^{-1}$) and 256 nm (177600 $dm^3\cdot mol^{-1}\cdot cm^{-1}$). While the band observed at 375 nm is due to the LMCT transition, the band at 970 nm is assignable to $^4T_{1g}$ (F) $\rightarrow$ $^4T_{2g}$ transition of high-spin Co^{II} center in an octahedral environment. In the $Pd^{II}Ni^{II}$ complex **8**, in addition to the two bands in the UV region (378 and 260 nm), two more bands are observed in the visible (550 nm) and in the near-IR region (985 nm). Figure S3 shows the absorption spectrum of complex **8** in acetonitrile. The bands observed at 985 nm (8 $dm^3\cdot mol^{-1}\cdot cm^{-1}$) and 550 nm (17 $dm^3\cdot mol^{-1}\cdot cm^{-1}$) are due to $^3A_{2g} \rightarrow {}^3T_{2g}$ and $^3A_{2g} \rightarrow {}^3T_{1g}$ (P) transitions of the six-coordinate nickel(II) center. We note that a third band expected for $^3A_{2g} \rightarrow {}^3T_{1g}$ transition is not observed. The $Pd^{II}Cu^{II}$ complex **9** exhibits a single d–d band at 700 nm (39.9 $dm^3\cdot mol^{-1}\cdot cm^{-1}$) in addition to the bands at

Table 3. Absorption and emission spectroscopic data for complexes **1**–**11**.[a]

	Absorption	Emission	
	λ_{max} [nm] (ε [dm^3·mol^{-1}·cm^{-1}])	λ_{max} [nm]	φ
1	409 (24700), 266 (129800), 221 (190500)		
2	407 (26300), 261 (144500), 222 (176000)	505	0.012
3	385 (27800), 261 (131000), 223 (183900)		
4	385 (27800), 261 (131000), 223 (183900)		
5	372 (32000), 261 (167000)		
6	374 (34200), 259 (163200)		
7	970 (16), 375 (36400), 256 (177600)		
8	985 (8), 550 (17), 378 (32500), 259 (157000)		
9	700 (40), 375 (34200), 258 (162000)		
10	406 (22400), 259 (166700), 219 (189700)	437	0.033
11	398 (21200), 264 (100900), 219 (179500)	443	0.005

[a] In acetonitrile.

375 and 258 nm (Figure S4). No d–d bands could be observed for the $Pd^{II}Mn^{II}$ and $Pd^{II}Fe^{II}$ complexes **5** and **6**, respectively.

Luminescence Spectra

The luminescence spectra of the mononuclear palladium complex **2**, the heterodinuclear $Pd^{II}Zn^{II}$ complex **10**, and the dipalladium(II) complex **11** were measured in acetonitrile solution at room temperature. Table 3 summarizes the emission spectral characteristics of the complexes, including their quantum yields. The mononuclear Pd^{II} complex on excitation at 400 nm exhibits a luminescence peak at 505 nm. In the $Pd^{II}Zn^{II}$ complex **10**, the luminescence peak is blue-shifted to 437 nm with increased intensity. On the other hand, for the dipalladium(II) complex **11**, considerable diminution of emission intensity occurs for the luminescence peak observed at 443 nm.

Spectrofluorimetric titrations carried out by adding incremental amounts of an acetonitrile solution of $Zn(OAc)_2·2H_2O$ to a solution of **2** containing 2 equiv. of sodium acetate in the same solvent, leading to the formation of **10**, is shown in Figure 4. The emission band of **2** at 505 nm (λ_{ex} = 400 nm) progressively gets quenched with the addition of zinc(II), whereas a new band appearing at 437 nm due to the formation of **10** progressively increases. The growth of the emission band at 437 nm was monitored as a function of the concentration of zinc acetate added. The inset in Figure 4 shows that the luminescence intensity reached its maximum when 1 equiv. of $Zn(OAc)_2·2H_2O$ was added.

A similar observation has been made for the spectrofluorimetric titration of **2** with palladium acetate (Figure 5). With the incremental addition of palladium acetate the band at 505 nm decreases, giving rise to a new band at 443 nm corresponding to the formation of the dipalladium complex **11**. Again, the growth of the 443 nm band was complete when 1 equiv. of palladium acetate was added. It has been established from additional measurements that the presence of 2 equiv. of sodium acetate is essential for the completion of the reactions. For instance, when titrations were carried out without adding sodium acetate, 2 equiv. of

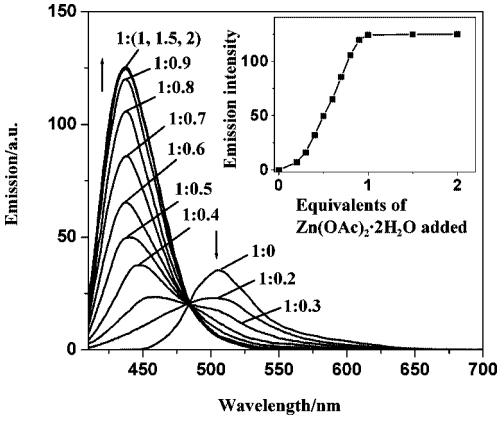

Figure 4. Spectrofluorimetric titration of a mixture of $[Pd(LH_2)][ClO_4]_2$ (**2**) (1×10^{-5} mol·dm^{-3}) and NaOAc (2×10^{-5} mol·dm^{-3}) with $Zn(OAc)_2·2H_2O$ in acetonitrile. The excitation wavelength used was 400 nm. The inset shows the variation of luminescence intensity with the number of equivalents of $Zn(OAc)_2·2H_2O$ added.

$M(OAc)_2$ were required for the completion of the reactions. Clearly, the role of the excess acetate is to provide a buffer effect to the liberated acetic acid in Reaction (1).

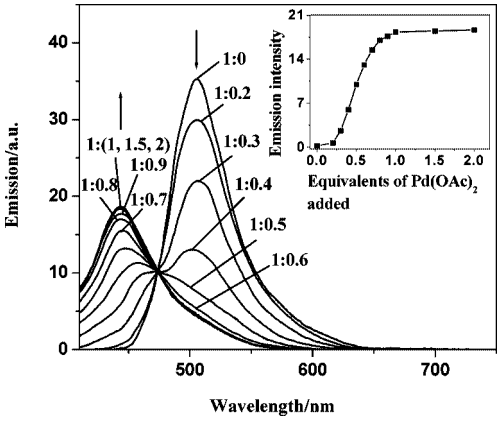

Figure 5. Spectrofluorimetric titration of a mixture of $[Pd(LH_2)][ClO_4]_2$ (**2**) (1×10^{-5} mol·dm^{-3}) and NaOAc (2×10^{-5} mol·dm^{-3}) with $Pd(OAc)_2$ in acetonitrile. The excitation wavelength used was 400 nm. The inset shows the variation of luminescence intensity with the number of equivalents of $Pd(OAc)_2$ added.

$$[Pd(LH_2)]^{2+} + M(OAc)_2 \rightleftharpoons [Pd(L)M]^{2+} + 2\ HOAc \quad (1)$$

In this context, it may be mentioned that relative to $[PdLZn]^{2+}$ the luminescence intensity of $[Zn_2L]^{2+}$ is seven times stronger.[26]

Proton NMR Spectra

Proton NMR spectroscopic studies were carried out for the diamagnetic complexes **1**–**4**, **10**, **11** in $(CD_3)_2SO$ and for the paramagnetic complexes **6**–**9** in CD_3CN. The observed chemical shifts along with the spectral assignments are given in the Experimental Section.

The spectral features exhibited by the mononuclear Rh^{III} complex **1** and Pd^{II} complex **2** are quite similar. The hydrogen-bonded protonated imine N–H···O is observed as a broad singlet at δ = 12.44 ppm for **1** and 12.22 ppm for **2**. Complex **1** exhibits a doublet for the N=CH resonance in the metal-free compartment at δ = 8.75 ppm (J = 14.8 Hz, 2 H), because of *trans* coupling between the NH and CH protons; however, for complex **2** this is observed as a singlet at δ = 8.80 ppm. The N=CH resonance in the metal-containing part appears as a singlet at δ = 8.06 ppm (for **1**) and 8.11 ppm (for **2**). The occurrence of the doublet at δ = 8.75 ppm in **1** can be alternatively argued as being due to the coupling of the CH=N proton with ^{103}Rh (I = 1/2). However, we have recently reported[27] that in the $[Ln(LH_2)(NO_3)_3]$-type diamagnetic lanthanide (La, Lu, and Y) complexes the CH=N resonances are observed as a doublet between 8.73 and 8.80 ppm and a singlet between 8.20 and 8.30 ppm. Significantly, while ^{89}Y (100%) is a spin 1/2 nucleus, neither La nor Lu have a I = 1/2 isotope, albeit for all three compounds the chemical shifts and splitting patterns are similar. It, therefore, appears more reasonable to us to conclude that the doublet arises because of *trans* coupling with the N–H proton. In the heterodinuclear $Rh^{III}Pd^{II}$ complexes **3**/**4**, the protons on the Rh-containing site are more shielded than the protons on the Pd-containing site, whereas in the $Pd^{II}Zn^{II}$ complex **10** the protons on the Pd site are more shielded than those on the Zn-containing site.

Studies on the paramagnetic ^1H NMR spectroscopic behavior of the heterodinuclear complexes **6**–**9** were carried out in CD_3CN solution. The $Pd^{II}Mn^{II}$ complex **5** could not be investigated as it readily decomposes in solution. The spectroscopic data for complexes **6**–**9** are given in the Experimental Section. In paramagnetic compounds, hyperfine-shifted resonances are observed due to interactions between nuclear spin and unpaired electron spins, in addition to the normal diamagnetic nuclear spin interactions. Electron and nuclear spin interactions occurring through bonds give rise to contact shift, while those occurring through space interactions give rise to dipolar or pseudocontact shift. Dipolar shift depends on the magnetic anisotropy of the system and the position in space of a given proton. The contribution of contact shift decreases rapidly with the increase of the number of bonds connecting the proton with the paramagnetic center. However, when the unpaired electron spin is delocalized the interaction remains significant for protons many bonds away from the metal center. For assignment of signals in paramagnetic compounds, measurement of longitudinal relaxation times (T_1) and transverse relaxation times (T_2) are particularly important. T_1 correlates proximity of proton to paramagnetic center, while $T_2 = 1/\pi(\text{fwh})$, where fwh is full width of a signal at its half-height, correlates line width to proximity of a proton to the paramagnetic site. Closer proximity of a proton to the metal center gives rise to shorter T_1 and broader line width.[28]

Figure 6 and Figure 7 show the ^1H NMR spectra of $Pd^{II}Co^{II}$ (**7**) and $Pd^{II}Ni^{II}$ (**8**) compounds, while the spectrum of $Pd^{II}Cu^{II}$ (**9**) is available as supporting information (Figure S5). The assignments of signals given in Table 4 (numbering scheme for protons is shown in Scheme 2) have been made from T_1 values, line widths, and integration of protons. The M···H distances ($R_{M\cdots H}$) have been estimated by using the relation $R_{M\cdots H} = R_{ref}(T_1/T_{ref})^{1/6}$, where R_{ref} and T_{ref} are the reference values and in the present case the 4-methyl group is treated as the reference. As compared in Table 4, there is good agreement between the $R_{M\cdots H}$ values

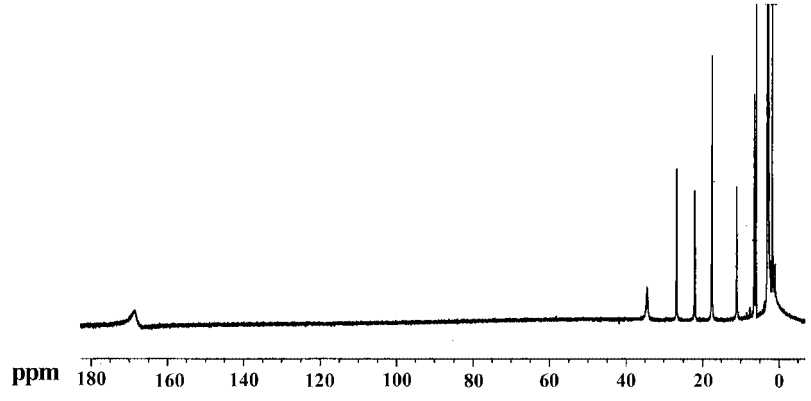

Figure 6. ^1H NMR spectrum of $[Pd^{II}LCo^{II}(H_2O)_2](ClO_4)_2$ (**7**) in CD_3CN.

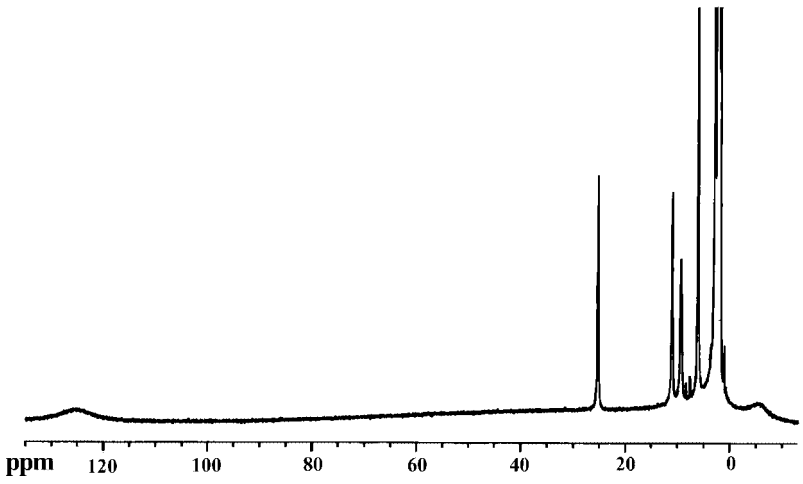

Figure 7. ^{1}H NMR spectrum of $[Pd^{II}LNi^{II}(H_2O)_2](ClO_4)_2$ (**8**) in CD_3CN.

Table 4. Peak positions, T_1 and T_2 values, proximity of H's to M, and assignments for compounds **7**–**9**.

	$Pd^{II}Co^{II}$ (**7**)					$Pd^{II}Ni^{II}$ (**8**)					$Pd^{II}Cu^{II}$ (**9**)				
Assign ment	δ [ppm]	T_1 [ms]	T_2[a] [ms]	$R_{Co\cdots H}$ [Å] X-ray	soln.[b]	δ [ppm]	T_1 [ms]	T_2[a] [ms]	$R_{Ni\cdots H}$ [Å][25] X-ray	soln.[b]	δ [ppm]	T_1 [ms]	T_2[a] [ms]	$R_{Cu\cdots H}$ [Å] X-ray	soln.[b]
a	6.09	11.53*	26.20	7.46*		2.96	10.90*	21.23	7.46*		3.08	14.05*	17.69	7.47*	
b	22.08	4.19	8.84		6.30	11.15	4.02	4.89	6.31	6.32	7.50	4.85	3.74	6.25	6.26
b′	11.09	1.28	7.96		5.17	9.42	1.25	3.31	5.18	5.20	22.64	1.66	0.29	5.18	5.23
c	26.73	2.55	9.80		5.80	25.53	2.68	5.13	5.88	5.90	7.96	3.29	6.63	5.81	5.86
c′	—					—			3.71		—			3.72	
d	17.60	5.59	8.85		6.61	6.14	4.92	5.68	6.49	6.53	5.19	6.81	5.52	6.49	6.62
d′	168.3	—	0.5		—	128.10	—	0.14	3.78	—	—			3.81	
e	6.58	9.88	13.26		7.27	2.60	9.65	6.92	7.34	7.30	1.21	12.04	8.84	7.11	7.28
e′	34.46	—	2.27		—	–5.0	—	0.27	3.15	—	–12.0	—	0.27	3.21	—

[a] $T_2 = 1/\pi$(fwh), fwh is full width at half height. [b] In solution, calculated $R_{M\cdots H} = R_{ref}(T_1/T_{ref})^{1/6}$, where R_{ref} and T_{ref} are reference (*) values.

obtained by the NMR method and those obtained from the X-ray structure determinations of the compounds $Pd^{II}Ni^{II}$ (**8**)[25] and $Pd^{II}Cu^{II}$ (**9**). The $Pd^{II}Co^{II}$ compound **7** may be considered as isostructural with the $Pd^{II}Ni^{II}$ compound **8** and on that basis the Co···H distances obtained from T_1 measurements are in good agreement with the Ni···H distances obtained from the X-ray structure.

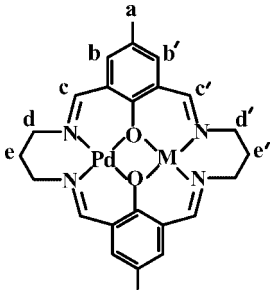

Scheme 2.

Electrochemistry

The electrochemical properties of complexes **7**–**9** have been studied in acetonitrile using platinum and glassy carbon electrodes. Figure 8 (a) shows the cyclic voltammogram and square-wave voltammogram of $Pd^{II}Cu^{II}$ complex **9**, which undergoes one electron reduction of copper(II). The redox potential ($E_{1/2}$) of the $Pd^{II}Cu^{II}/Pd^{II}Cu^{I}$ couple, as obtained from CV, is –108 mV and the peak-to-peak separation is 60 mV versus Ag/AgCl. The $E_{1/2}$ obtained from square-wave voltammetry is –104 mV. In the potential range 0–1.5 V, an irreversible oxidation occurs for the $Pd^{II}Cu^{II}$

compound at 760 mV, which, however, is not observed for the $Pd^{II}Ni^{II}$ and $Pd^{II}Co^{II}$ complexes. It appears that this oxidation is not due to the formation of the ligand-based phenoxide radical because a similar observation has not been made for compounds **7** and **8**. As oxidation to the Pd^{III} state seems unlikely, the formation of $Pd^{II}Cu^{III}$ species appears to be more plausible. As shown in Figure 8 (b), the $Pd^{II}Ni^{II}$ complex **8** also undergoes near-reversible reduction with $E_{1/2}$ = –803 mV for the couple $Pd^{II}Ni^{II}/Pd^{II}Ni^{I}$ and ΔE_p = 74 mV. In contrast, the $Pd^{II}Co^{II}$ complex **7** undergoes irreversible reduction for Co^{II} at $E_{p,c}$ = –780 mV.

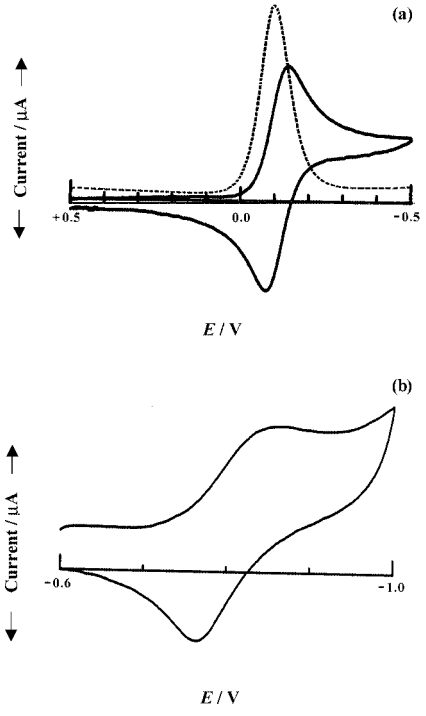

Figure 8. (a) Cyclic and square-wave voltammogram of $[Pd^{II}LCu^{II}](ClO_4)_2$ (**9**) and (b) cyclic voltammogram of $[Pd^{II}LNi^{II}(H_2O)_2](ClO_4)_2$ (**8**) in acetonitrile.

Conclusions

Using $[Pb(LH_2)](ClO_4)_2$ as the precursor macrocyclic complex, mononuclear $[Pd(LH_2)_2](ClO_4)_2$ and $[Rh(LH_2)Cl_2](ClO_4)\cdot 3H_2O$ complexes have been prepared, which in turn have been used to produce 4d–3d heterobimetallic complexes, viz. $[Pd(L)M(H_2O)_2](ClO_4)_2$ (M = Mn, Fe, Co, Ni), $[Pd(L)Cu](ClO_4)_2$, and $[Pd(L)Zn(H_2O)](ClO_4)_2\cdot H_2O$ as well as $[RhCl_2(L)Pd](PF_6)$ and $[Pd_2L](ClO_4)_2$. The crystal structures of the $Rh^{III}Pd^{II}$ and $Pd^{II}Cu^{II}$ complexes have been determined. Proton NMR spectroscopic measurements have been carried out for the paramagnetic compounds and M···H (ligand proton) distances estimated from the relaxation time (T_1) values agreed fairly well with those obtained from X-ray studies. The mononuclear palladium(II) complex, which exhibits photoluminescence, during titration with $Pd(OAc)_2$ undergoes blue-shift of λ_{em} and diminution of luminescence intensity because of the formation of the $[Pd_2L]^{2+}$ complex. On the other hand, the formation of $[Pd(L)Zn]^{2+}$ species, although it leads to a similar blue-shift of λ_{em}, is accompanied by augmentation of luminescence intensity. The $Pd^{II}Cu^{II}$ complex undergoes facile reversible electrochemical reduction to $Pd^{II}Cu^{I}$ with $E_{1/2}$ = –106 mV and irreversible oxidation to $Pd^{III}Cu^{II}$ at $E_{p,a}$ = 760 mV. The $Pd^{II}Ni^{II}$ complex also undergoes one-electron reversible reduction to $Pd^{II}Ni^{I}$ with $E_{1/2}$ = –803 mV, although no oxidation occurs up to +1.5 V. The redox behavior of the $Pd^{II}Co^{II}$ complex in the positive potential range (0 to +1.5 V) is again featureless, albeit reduction of the Co^{II} center takes place irreversibly at $E_{p,c}$ = –780 mV.

Experimental Section

Materials: Reagent grade chemicals obtained from commercial sources were used as received. Solvents were purified and dried according to standard methods.[29] 2,6-Diformyl-4-methylphenol was prepared according to the literature method.[30] The precursor complex $[Pb(LH_2)](ClO_4)_2$ was synthesized as reported earlier.[23]

Preparation of the Complexes

CAUTION: All the perchlorate salts reported in this study are potentially explosive and therefore should be handled with care.

Mononuclear Complexes $[Rh(LH_2)Cl_2](ClO_4)\cdot 3H_2O$ (1), $[Pd(LH_2)](ClO_4)_2$ (2): A methanol solution (10 mL) of the metal chloride salts $RhCl_3\cdot xH_2O$ or $Na_2[PdCl_4]$ (1 mmol) and an acetonitrile solution (10 mL) of $NaClO_4\cdot xH_2O$ (550 mg, 4 mmol) were added to a boiling acetonitrile solution (50 mL) of $[Pb(LH_2)](ClO_4)_2$ (810 mg, 1 mmol). The color of the solution changed from yellow to wine red (for Rh) or orange (for Pd). The solution was refluxed for 12 h. After removal of the precipitated $PbCl_2$ by filtration, the filtrate was concentrated on a water bath to a volume of about 20 mL. The yellow or orange crystalline products that deposited on standing were collected by filtration and washed with methanol and diethyl ether.

$[Rh(LH_2)Cl_2](ClO_4)\cdot 3H_2O$ (1): Orange crystalline compound. Yield: 450 mg (62%). MS (ESI+ in CH_3CN): *m*/*z* = 577 $[Rh(Cl_2)(LH_2)]^+$ (100%), 641 $[Rh(Cl)(ClO_4)(LH_2)]^+$ (50%). ^1H NMR [300 MHz, $(CD_3)_2SO$, 25 °C]: δ = 12.44 (s, 2 H, N–H···O), 8.75 (d, J = 14.8 Hz, 2 H, CH=N, metal-free site), 8.06 (s, 2 H, CH=N, metal-containing site), 7.57 (s, 2 H, Ar, metal-free site), 7.44 (s, 2 H, Ar, metal-containing site), 4.10 (s, 4 H, α-CH_2, metal-free site), 4.02 (s, 4 H, α-CH_2, metal-containing site), 2.21 (s, 6 H, CH_3), 2.09 (m, 4 H, β-CH_2) ppm. IR (KBr [cm^{-1}]): $\tilde{\nu}$ = 3459 br, 3147 w, 3080 w, 2919 w, 1650 s, 1550 s, 1469 m, 1445 m, 1357 m, 1279 m, 1237 m, 1122 s, 1084 s, 870 w, 823 w, 769 w, 628 m, 561 w, 487 w. $C_{24}H_{34}Cl_3N_4O_9Rh$ (731.82): calcd. C 39.39, H 4.68, N 7.66; found C 39.09, H 4.58, N 7.71.

$[Pd(LH_2)](ClO_4)_2$ (2): Yellow crystalline compound. Yield: 510 mg (72%). MS (ESI+ in CH_3CN): *m*/*z* = 611 $[Pd(LH_2)(ClO_4)]^+$ (10%), 256 $[Pd(LH_2)]^{2+}$ (100%). ^1H NMR [300 MHz, $(CD_3)_2SO$, 25 °C]: δ = 12.23 (s, 2 H, N–H···O), 8.80 (s, 2 H, CH=N, metal-free site), 8.11 (s, 2 H, CH=N, metal-containing site), 7.78 (s, 2 H, Ar, metal-free site), 7.63 (s, 2 H, Ar, metal-containing site), 3.98 (s, 4 H, α-CH_2, metal-free site), 3.85 (s, 4 H, α-CH_2, metal-containing site), 2.27 (s, 6 H, CH_3), 2.10 (s, 4 H, β-CH_2) ppm. IR (KBr [cm^{-1}]): $\tilde{\nu}$ = 3449 br, 3143 w, 3078 w, 2921 w, 1650 s, 1552 s, 1477 m, 1450 m, 1351 m, 1291 w, 1236 w, 1233 w, 1217 w, 1082 s, 1014 s, 861 w, 822 m, 624 m, 519 w. $C_{24}H_{28}Cl_2N_4O_{10}Pd$ (709.83): calcd. C 40.61, H 3.98, N 7.89; found C 40.52, H 4.05, N 7.87.

$[RhCl_2(L)Pd](ClO_4)\cdot 0.5H_2O$ (3): A methanol solution (15 mL) of $Na_2[PdCl_4]$ and an acetonitrile solution (15 mL) of triethylamine (40 mg, 0.4 mmol) were slowly added to an acetonitrile solution (15 mL) of compound **1** (150 mg, 0.2 mmol) with stirring. The resulting orange solution was refluxed for 4 h after which it was filtered. The filtrate was concentrated on a water bath to a volume of about 10 mL and then slowly cooled to room temperature. On standing for several hours a crystalline red-orange compound deposited, which was filtered and washed with methanol and diethyl ether. Yield: 110 mg (69%). MS (ESI+ in CH_3CN): *m*/*z* = 682.9 $[Rh(Cl_2)(L)Pd]^+$ (100%). ^1H NMR [300 MHz, $(CD_3)_2SO$, 25 °C]: δ = 8.19 (s, 2 H, CH=N, Pd site), 8.13 (s, 2 H, CH=N, Rh site), 7.65 (s, 2 H, Ar, Pd site), 7.62 (s, 2 H, Ar, Rh site), 3.94 (s, 4 H, α-CH_2, Pd site), 3.74 (s, 4 H, α-CH_2, Rh site), 2.27 (s, 6 H, CH_3), 2.07 (s, 4 H, β-CH_2) ppm. IR (KBr [cm^{-1}]): $\tilde{\nu}$ = 3422 br, 3065 w, 2924 w, 2866 w, 1630 s, 1569 s, 1468 m, 1435 m, 1367 w, 1330 s, 1279 m, 1248 m, 1089 s, 950 w, 833 m, 754 m, 624 m, 520 w, 439 w. $C_{24}H_{27}Cl_3N_4O_{6.5}PdRh$ (790.98): calcd. C 36.44, H 3.44, N 7.08; found C 36.52, H 3.69, N 6.86.

$[RhCl_2(L)Pd](PF_6)$ (4): Solid ammonium hexafluorophosphate (150 mg) was added to an acetonitrile solution (15 mL) of compound **3** (60 mg, 0.07 mmol), and the orange solution turned to red-orange. The solution was filtered and the filtrate was slowly concentrated on a hot plate. The product that deposited as red-orange crystals was collected by filtration. Crystals suitable for X-ray diffraction studies were obtained by diffusing diethyl ether into an acetonitrile solution of the compound. Yield: 40 mg (72%). MS (ESI+ in CH_3CN): *m*/*z* = 682.9 $[Rh(Cl_2)(L)Pd]^+$ (100%). IR (KBr [cm^{-1}]): $\tilde{\nu}$ = 2942 w, 1629 s, 1571 s, 1469 m, 1433 m, 1330 m, 1277 w, 1247 m, 1198 w, 1117 m, 958 w, 839 s, 753 m, 646 w, 555 m, 518 m, 407 w. $C_{24}H_{26}Cl_2F_6N_4O_2PPdRh$ (827.69): calcd. C 34.82, H 3.17, N 6.77; found C 34.96, H 3.26, N 6.64. The ^1H NMR spectrum of **4** is identical to that of **3**.

Heterodinuclear $[Pd^{II}(L)M^{II}(H_2O)_n](ClO_4)_2$ [M = Mn, Fe, Co, Ni, Cu, Zn] Complexes (5–10): A generalized procedure for preparing these complexes is given. An acetonitrile solution (15 mL) of $M(ClO_4)_2\cdot 6H_2O$ ($M = Mn^{II}$, Fe^{II}, Co^{II}, Ni^{II}, Zn^{II}) was added to an acetonitrile solution (30 mL) of compound **2** (140 mg, 0.2 mmol). The resulting solution was then slowly treated with an acetonitrile solution (15 mL) of triethylamine (40 mg, 0.4 mmol). After refluxing the solution for 2 h, it was concentrated on a water bath to a volume of about 10 mL. Preparation of the $Pd^{II}Mn^{II}$, $Pd^{II}Fe^{II}$, and $Pd^{II}Co^{II}$ complexes was carried out under nitrogen. The product that deposited in crystalline form on keeping the solution at room temperature was collected by filtration and washed with methanol and diethyl ether.

$[Pd(L)Mn(H_2O)_2](ClO_4)_2$ (5): Light orange crystalline compound. Yield: 110 mg (73%). Satisfactory mass spectrum could not be obtained. IR (KBr [cm^{-1}]): $\tilde{\nu}$ = 3410 br, 2929 m, 2851 w, 1633 s, 1563 s, 1459 w, 1434 m, 1412 m, 1324 m, 1114 s, 1087 s, 966 w, 825 s, 759 w, 622 m, 561 w, 501 w. $C_{24}H_{30}Cl_2MnN_4O_{12}Pd$ (798.98): calcd. C 36.09, H 3.79, N 7.01; found C 36.17, H 3.79, N 7.09.

$[Pd(L)Fe(H_2O)_2](ClO_4)_2$ (6): Red-brown crystalline compound. Yield: 100 mg (67%). MS (ESI+ in CH_3CN): *m*/*z* = 662.9 $[Pd(L)Fe(ClO_4)]^+$ (9%) and 283 $[Pd(L)Fe]^{2+}$ (100%). ^1H NMR (300 MHz, CD_3CN, 25 °C): δ = 80.21 (4 H), 35.84 (2 H), 20.83 (2 H), 10.90 (2 H), 7.91 (2 H), 4.44 (2 H), 4.22 (2 H), 3.79 (6 H), 1.23 (2 H) ppm. IR (KBr [cm^{-1}]): $\tilde{\nu}$ = 3456 br, 3169 w, 2921 w, 2856 w, 1635 s, 1566 s, 1440 m, 1413 w, 1317 m, 1277 m, 1243 w, 1196 w, 1106 s, 959 w, 924 w, 821 m, 755 w, 622 m, 519 w. $C_{24}H_{30}Cl_2FeN_4O_{12}Pd$ (799.69): calcd. C 36.05, H 3.78, N 7.01; found C 36.29, H 3.78, N 7.10.

$[Pd(L)Co(H_2O)_2](ClO_4)_2$ (7): Red-orange crystalline compound. Yield: 120 mg (75%). MS (ESI+ in CH_3CN): *m*/*z* = 667.9 $[Pd(L)Co(ClO_4)]^+$ (11%) and 284.5 $[Pd(L)Co]^{2+}$ (100%). ^1H NMR (300 MHz, CD_3CN, 25 °C): δ = 168.31 (4 H), 34.46 (2 H), 26.73 (2 H), 22.07 (2 H), 17.6 (4 H), 11.09 (2 H), 6.58 (2 H), 6.09 (6 H) ppm. IR (KBr [cm^{-1}]): $\tilde{\nu}$ = 3433 br, 2923 w, 2852 w, 1634 s, 1563 s, 1555 m, 1461 w, 1438 m, 1412 m, 1326 s, 1279 w, 1242 w, 1195 w, 1114 s, 1087 s, 966 w, 922 w, 823 m, 759 w, 624 m, 519 w. $C_{24}H_{30}Cl_2CoN_4O_{12}Pd$ (802.78): calcd. C 35.91, H 3.77, N 6.98; found C 35.84, H 3.72, N 7.04.

$[Pd(L)Ni(H_2O)_2](ClO_4)_2$ (8): Light green crystalline compound. Yield: 120 mg (75%). MS (ESI+ in CH_3CN): *m*/*z* = 666.9 $[Pd(L)Ni(ClO_4)]^+$ (8%) and 285 $[Pd(L)Ni]^{2+}$ (100%). ^1H NMR (300 MHz, CD_3CN, 25 °C): δ = 128.10 (4 H), 25.53 (2 H), 11.15 (2 H), 9.42 (2 H), 6.14 (4 H), 2.96 (6 H), 2.60 (2 H), –5.00 (2 H) ppm. IR (KBr [cm^{-1}]): $\tilde{\nu}$ = 3428 br, 2909 w, 2851 w, 1643 s, 1618 s, 1565 s, 1461 m, 1438 m, 1413 m, 1326 s, 1283 m, 1243 w, 1195 w, 1121 s, 1092 sh, 1052 sh, 965 w, 922 w, 823 m, 760 w, 621 m, 520 w. $C_{24}H_{30}Cl_2N_4NiO_{12}Pd$ (800.54): calcd. C 36.01, H 3.78, N 6.99; found C 35.99, H 3.85, N 6.81.

$[Pd(L)Cu](ClO_4)_2$ (9): Deep green crystalline compound. Yield: 130 mg (86%). MS (ESI+ in CH_3CN): *m*/*z* = 671.9 $[Pd(L)Cu(ClO_4)]^+$ (10%) and 287.5 $[Pd(L)Cu]^{2+}$ (100%). ^1H NMR (300 MHz, CD_3CN, 25 °C): δ = 22.64 (2 H), 7.96 (2 H), 7.50 (2 H), 5.19 (4 H), 3.08 (6 H), 1.21 (2 H), –12.00 (2 H) ppm. IR (KBr [cm^{-1}]): $\tilde{\nu}$ = 2922 w, 2859 w, 1632 s, 1572 s, 1468 w, 1436 m, 1419 m, 1326 s, 1283 m, 1245 m, 1198 m, 1094 s, 961 w, 935 w, 826 m, 756 m, 620 m, 518 w. $C_{24}H_{26}Cl_2CuN_4O_{10}Pd$ (771.36): calcd. C 37.37, H 3.39, N 7.26; found C 37.37, H 3.27, N 7.42.

$[Pd(L)Zn(H_2O)](ClO_4)_2\cdot H_2O$ (10): Yellow crystalline compound. Yield: 110 mg (69%). MS (ESI+ in CH_3CN): *m*/*z* = 672.9 $[Pd(L)Zn(ClO_4)]^+$ (12%) and 288 $[Pd(L)Zn]^{2+}$ (100%). ^1H NMR [300 MHz, $(CD_3)_2SO$, 25 °C]: δ = 8.45 (s, 2 H, CH=N, Zn site), 8.10 (s, 2 H, CH=N, Pd site), 7.49 (s, 2 H, Ar, Zn site), 7.46 (s, 2 H, Ar, Pd site), 3.94 (s, 4 H, α-CH_2, Zn site), 3.82 (s, 4 H, α-CH_2, Pd site), 2.26 (s, 6 H, CH_3), 2.06 (s, 4 H, β-CH_2) ppm. IR (KBr [cm^{-1}]): $\tilde{\nu}$ = 3410 br, 2927 m, 2866 w, 1637 s, 1564 s, 1439 m, 1414 m, 1366 w, 1280 m, 1243 m, 1197 w, 1087 s, 969 w, 937 w, 890 w, 825 m, 761 m, 627 m, 572 w, 506 w. $C_{24}H_{30}Cl_2N_4O_{12}PdZn$ (809.23): calcd. C 35.62, H 3.74, N 6.92; found C 35.80, H 3.78, N 7.01.

Homodinuclear $[Pd(L)Pd](ClO_4)_2$ Complex (11): A methanol solution (15 mL) of $Na_2[PdCl_4]$ (60 mg, 0.2 mmol) and an acetonitrile solution (5 mL) of triethylamine (40 mg, 0.4 mmol) were added successively to an acetonitrile solution (30 cm^3) of $[Pd(LH_2)](ClO_4)_2$ (140 mg, 0.2 mmol). The mixture was refluxed for 2 h, during which time NaCl was precipitated and removed by filtration. $NaClO_4$ (50 mg) was added to the filtrate and the volume of the solution was reduced to about 15 mL on a rotary evaporator. After filtration, the filtrate was kept on a hot plate for slow evaporation and eventually orange crystals were deposited. The product was collected by filtration and washed with cold methanol and diethyl ether. Yield: 120 mg (75%). MS (ESI+ in CH_3CN): *m*/*z* = 714.9 $[Pd(L)Pd(ClO_4)]^+$ (8%) and 309 $[Pd(L)Pd]^{2+}$ (100%). ^1H NMR [300 MHz, $(CD_3)_2SO$, 25 °C]: δ = 8.16 (s, 4 H, CH=N), 7.77 (s, 4 H, Ar), 3.68 (s, 8 H, α-CH_2), 2.30 (s, 6 H, CH_3), 2.03 (s, 4 H, β-CH_2) ppm. IR (KBr [cm^{-1}]): $\tilde{\nu}$ = 2930 w, 2848 w, 1625 s, 1571 s, 1469 m, 1329 s, 1283 w, 1246 w, 1097 m, 1087 s, 955 m, 879 w, 838 m, 751 m, 620 m, 512 w. $C_{24}H_{26}Cl_2N_4O_{10}Pd_2$ (814.23): calcd. C 35.40, H 3.22, N 6.88; found C 35.59, H 3.18, N 6.91.

Physical Measurements: Elemental C, H, and N analyses were performed with a Perkin–Elmer 2400II elemental analyzer. The ^1H

NMR (300 MHz) spectra were performed in CD_3CN (for **6**–**9**) and $(CD_3)_2SO$ solutions (for **1**–**4**, **10**, **11**) with a Bruker Avance DPX-300 spectrometer. Longitudinal relaxation times (T_1) were measured by the inversion recovery method. IR spectra were recorded using KBr disks with a FTIR Nexus Nicolet spectrometer using KBr disks. The electronic spectra of **1**–**11** in acetonitrile were measured in the range 250–1100 nm using Perkin–Elmer Lambda 950 spectrophotometer. Emission spectral measurements were carried out with a Perkin–Elmer LS55 luminescence spectrometer with 10^{-5} mol·dm^{-3} acetonitrile solutions. Emission quantum yields (φ) were measured at room temperature in acetonitrile solution relative to perylene as the standard.[31] The quantum yields were calculated using the relation[32]

$$\varphi = \varphi_{std}(A_{std}/A)(I/I_{std})(\eta^2/\eta^2_{std})$$

where A, I, and η refer to absorbance, integrated emission intensity, and solution refractive index, respectively. Electrospray ionization mass spectra (ESI-MS) of compounds **1**–**11** were measured in acetonitrile with a Micromass Qtof YA263 mass spectrometer. The electrochemical measurements were carried out with a BAS 100B electrochemistry system using a three-electrode assembly comprising a Pt or glassy carbon working electrode, Pt auxiliary electrode, and an aqueous Ag/AgCl reference electrode. The measurements (CV) were carried out at 25 °C under nitrogen in acetonitrile solution of complexes **7**–**9** (about 1 mmol·dm^{-3}) with tetraethylammonium perchlorate (TEAP) (0.1 mol·dm^{-3}) as the supporting electrolyte. The reference electrode was separated from the bulk electrolyte by a salt bridge containing 0.1 mmol·dm^{-3} TEAP in acetonitrile/water (1:1). The potentials measured were automatically compensated for the iR drop and under this condition the ferrocene/ferrocenium couple occurred at 430 mV.

X-ray Crystallography: The crystal structure analyses were carried out for compounds **4** and **9**, whose intensity data were collected at 293 K and 203 K, respectively with a Bruker AXS P4 diffractometer using graphite-monochromated Mo-K_α radiation (λ = 0.71073 Å). Crystal data and details of structure determinations are summarized in Table 5. The intensity data were corrected for Lorentz polarization effects and semiempirical absorption corrections were made from ψ-scans. The structures were solved by direct and Fourier methods and refined by full-matrix least-squares based on F^2 using SHELXTL.[33] The non-hydrogen atoms were refined anisotropically, while the hydrogen atoms were placed at the geometrically calculated positions with fixed isotropic thermal parameters.

Table 5. Crystallographic data for $[RhCl_2(L)Pd][PF_6]$ (**4**) and $[Pd(L)Cu](ClO_4)_2$ (**9**).

	4	**9**
Empirical formula	$C_{24}H_{26}Cl_2F_6N_4O_2PdRh$	$C_{24}H_{26}Cl_2CuN_4O_{10}Pd$
Formula mass	827.67	770.92
Crystal size [mm]	0.42×0.32×0.24	0.58×0.52×0.40
Crystal system	monoclinic	monoclinic
Space group	$P2_1/c$	$P2_1/n$
a [Å]	12.583(5)	7.2680(19)
b [Å]	17.446(2)	8.9890(13)
c [Å]	13.867(3)	20.738(5)
α [°]	90	90
β [°]	109.16(2)	92.30(2)
γ [°]	90	90
V [Å^3]	2875.5(13)	1353.8(5)
Z	4	2
D [g·cm^{-3}]	1.912	1.892
T [K]	293(2)	203(2)
λ [Å]	0.71073	0.71073
μ [mm^{-1}]	1.511	1.713
Measured/observed reflections	7944/6577	4316/3110
Parameters refined	371	187
Final R indices	R_1[a] = 0.0331,	R_1[a] = 0.0591,
[$I > 2\sigma(I)$]	wR_2[b] = 0.0735	wR_2[b] = 0.1779
R indices	R_1 = 0.0505,	R_1 = 0.0761,
(all data)	wR_2 = 0.0830	wR_2 = 0.1825

[a] $R_1(F) = \Sigma||F_o| - |F_c||/\Sigma|F_o|$. [b] $wR_2(F^2) = [\Sigma w(F_o^2 - F_c^2)^2/\Sigma w(F_o^2)^2]^{1/2}$.

CCDC-293271 and -293272 contain the supplementary crystallographic data for this paper. These data can be obtained free of charge from The Cambridge Crystallographic Data Centre via www.ccdc.cam.ac.uk/data_request/cif.

Supporting Information (see footnote on the first page of this article): Electrospray ionization mass spectra (ESI-MS+) of $[Pd^{II}(L)Cu^{II}](ClO_4)_2$ (**9**) in acetonitrile (Figure S1), absorption spectrum of compounds **7**–**9** (Figures S2–S4), and ^{1}H NMR spectrum of **9** in CD_3CN (Figure S5).

[1] N. H. Pilkington, R. Robson, *Aust. J. Chem.* **1970**, *23*, 2225–2236.

[2] a) H. Okawa, S. Kida, *Inorg. Nucl. Chem. Lett.* **1971**, *7*, 751–754; b) H. Okawa, S. Kida, *Bull. Chem. Soc. Jpn.* **1972**, *45*, 1759–1770.

[3] a) B. F. Hoskins, G. A. Williams, *Aust. J. Chem.* **1975**, *28*, 2607–2614; b) B. F. Hoskins, N. J. McLeod, H. A. Schaap, *Aust. J. Chem.* **1976**, *29*, 515–521.

[4] A. N. Addision, *Inorg. Nucl. Chem. Lett.* **1976**, *12*, 899–903.

[5] a) R. R. Gagne, C. A. Koval, T. J. Smith, *J. Am. Chem. Soc.* **1977**, *99*, 8367–8368; b) R. R. Gagne, C. A. Koval, T. J. Smith, M. C. Cimolino, *J. Am. Chem. Soc.* **1979**, *101*, 4571–4580.

[6] a) C. L. Spiro, S. E. Lambert, T. J. Smith, E. N. Duesler, R. R. Gagne, D. N. Hendrickson, *Inorg. Chem.* **1981**, *20*, 1229–1237; b) R. C. Long, D. N. Hendrickson, *J. Am. Chem. Soc.* **1983**, *105*, 1513–1521.

[7] a) S. K. Mandal, K. Nag, *J. Chem. Soc., Dalton Trans.* **1983**, 2429–2434; b) S. K. Mandal, K. Nag, *J. Chem. Soc., Dalton Trans.* **1984**, 2141–2149; c) S. K. Mandal, B. Adhikary, K. Nag, *J. Chem. Soc., Dalton Trans.* **1986**, 1175–1180.

[8] a) S. K. Mandal, L. K. Thompson, K. Nag, J.-P. Charland, E. J. Gabe, *Inorg. Chem.* **1987**, *26*, 1391–1395; b) S. K. Mandal, L. K. Thompson, K. Nag, J.-P. Charland, E. J. Gabe, *Can. J. Chem.* **1987**, *65*, 2815–2823; c) S. K. Mandal, L. K. Thompson, M. J. Newlands, E. J. Gabe, K. Nag, *Inorg. Chem.* **1990**, *29*, 1324–1327.

[9] a) P. Zanello, S. Tamburini, P. A. Vigato, G. A. Mazzocchin, *Coord. Chem. Rev.* **1987**, *77*, 165–273; b) P. A. Vigato, S. Tamburini, D. E. Fenton, *Coord. Chem. Rev.* **1990**, *106*, 25–170; c) P. Guerriero, S. Tamburini, P. A. Vigato, *Coord. Chem. Rev.* **1995**, *139*, 17–243.

[10] F. Lacroix, O. Kahn, F. L. Theobald, J. Leory, C. Wakselman, *Inorg. Chim. Acta* **1988**, *142*, 129–134.

[11] a) K. Brychcy, K. Dragger, K.-J. Jens, M. Tilset, U. Behrens, *Chem. Ber.* **1994**, *127*, 465–476; b) K. Brychcy, K.-J. Jens, M. Tilset, U. Behrens, *Chem. Ber.* **1994**, *127*, 991–995; c) K. Brychcy, K. Dragger, K.-J. Jens, M. Tilset, U. Behrens, *Chem. Ber.* **1994**, *127*, 1817–1826.

[12] a) L. K. Thompson, S. K. Mandal, S. S. Tandon, J. N. Bridson, M. K. Park, *Inorg. Chem.* **1996**, *35*, 3117–3125; b) S. K. Mandal, L. K. Thompson, M. J. Newlands, E. J. Gabe, *Inorg. Chem.* **1989**, *28*, 3707–3713.

[13] a) K. K. Nanda, L. K. Thompson, J. N. Bridson, K. Nag, *J. Chem. Soc., Chem. Commun.* **1994**, 1337–1338; b) K. K. Nanda, R. Das, L. K. Thompson, K. Venkatsubramanian, P. Paul, K. Nag, *Inorg. Chem.* **1994**, *33*, 1188–1193; c) K. K. Nanda, R. Das, L. K. Thompson, K. Venkatsubramanian, K.

Nag, *Inorg. Chem.* **1994**, *33*, 5934–5939; d) S. K. Dutta, R. Werner, U. Flörke, S. Mohanta, K. K. Nanda, W. Haase, K. Nag, *Inorg. Chem.* **1996**, *35*, 2292–2300; e) S. Mohanta, K. K. Nanda, L. K. Thompson, U. Flörke, K. Nag, *Inorg. Chem.* **1998**, *37*, 1465–1472.
[14] B. Bosnich, *Inorg. Chem.* **1999**, *38*, 2554–2562 and references cited therein.
[15] a) A. Asokan, B. Verghese, P. T. Manoharan, *Inorg. Chem.* **1999**, *38*, 4393–4399; b) S. Mohanta, B. Adhikary, S. Baitalik, K. Nag, *New J. Chem.* **2001**, *25*, 1466–1471.
[16] a) A. J. Atkins, A. J. Blake, M. Schröder, *J. Chem. Soc., Chem. Commun.* **1993**, 353–355; b) A. J. Atkins, D. Black, A. J. Blake, A. Marin-Becerra, S. Parsons, L. Rez-Ramirez, M. Schröder, *Chem. Commun.* **1996**, 457–464 and references cited therein; c) D. Black, A. J. Blake, R. L. Finn, L. F. Lindoy, A. Nezhdali, G. Rougnaghi, P. A. Tasker, M. Schröder, *Chem. Commun.* **2002**, 340–341.
[17] P. A. Vigato, S. Tamburini, *Coord. Chem. Rev.* **2004**, *248*, 1717–2128.
[18] N. Wheatley, P. Kalk, *Chem. Rev.* **1999**, *99*, 3379–3420.
[19] K. Severin, *Chem. Eur. J.* **2002**, *8*, 1514–1518.
[20] D. Karshtedt, A. T. Bell, T. D. Tilley, *Organometallics* **2003**, *22*, 2855–2861.
[21] a) R. W. J. Scott, A. K. Datye, R. M. Crooks, *J. Am. Chem. Soc.* **2003**, *125*, 3708–3709; b) Y. Mizukoshi, T. Fujimoto, Y. Nagata, R. Oshima, Y. Maeda, *J. Phys. Chem. B* **2000**, *104*, 6028–6032; c) R. W. J. Scott, O. M. Wilson, R. M. Crooks, *Chem. Mater.* **2004**, *16*, 5682–5688; d) R. W. J. Scott, O. M. Wilson, S. K. Oh, E. A. Kenik, R. M. Crooks, *J. Am. Chem. Soc.* **2004**, *126*, 15583–15591; e) R. W. J. Scott, C. Sivadinarayana, O. M. Wilson, Z. Yan, D. W. Goodman, R. M. Crooks, *J. Am. Chem. Soc.* **2005**, *127*, 1380–1381.
[22] A. J. Blake, T. I. Hyde, R. S. E. Smith, M. Schröder, *J. Chem. Soc., Chem. Commun.* **1986**, 334–336.
[23] B. Dutta, B. Adhikary, P. Bag, U. Flörke, K. Nag, *J. Chem. Soc., Dalton Trans.* **2002**, 2760–2767.
[24] B. Dutta, P. Bag, K. Nag, *New J. Chem.* **2005**, *29*, 1182–1188.
[25] P. Starynowicz, J. Lisowski, *Chem. Commun.* **1999**, 769–770.
[26] B. Dutta, P. Bag, U. Flörke, K. Nag, *Inorg. Chem.* **2005**, *44*, 147–157.
[27] P. Bag, U. Flörke, K. Nag, *Dalton Trans.* **2006**, 3236–3248.
[28] a) I. Bertini, P. Turano, A. Vila, *Chem. Rev.* **1993**, *93*, 2833–2932; b) I. Bertini, C. Luchinat, *NMR of Paramagnetic Substances*, Elsevier, Amsterdam, **1996**.
[29] D. D. Perrin, W. L. Armarego, D. R. Perrin, *Purification of Laboratory Chemicals*, 2nd ed., Pergamon, Oxford, **1980**.
[30] a) R. R. Gagne, C. L. Spiro, T. J. Smith, C. A. Hamann, W. R. Thies, A. K. Shiemke, *J. Am. Chem. Soc.* **1981**, *103*, 4073–4081; b) F. Ullmann, K. Brittner, *Ber. Dtsch. Chem. Ges.* **1909**, *42*, 2539–2548.
[31] H. Du, R. A. Fuh, J. Li, A. Corkan, J. S. Lindsay, *Photochem. Photobiol.* **1998**, *68*, 141–142.
[32] J. Van Houten, R. J. Watts, *J. Am. Chem. Soc.* **1976**, *98*, 4853–4858.
[33] Bruker, *SHELXTL* (Version 6.10), Bruker AXS Inc., Madison, WI, USA, **2002**.

Received: May 3, 2006
Published Online: August 21, 2006

